Materials Science and Engineering A 391 (2005) 210–220

www.elsevier.com/locate/msea

Surface oxidation kinetics of Cr film by Nd-YAG laser

Jianshe Lian[a], Qizhi Dong[a,b], Zuoxing Guo[a], Qing Xu[a], Jing Yang[a], Jiandong Hu[a,*], Qingfeng Guan[a], Bo Chen[b]

[a] *The Key Lab of Automobile Materials, Ministry of Education, College of Materials Science and Engineering, Jilin University, Changchun 130025, PR China*

[b] *State Key Lab of Applied Optics, Changchun 130025, PR China*

Received 5 December 2003; received in revised form 25 August 2004; accepted 31 August 2004

Abstract

Surface microstructures of Cr films by Nd-YAG laser oxidation and annealing oxidation were studied by SEM, FESEM, AFM and XRD. Cr films with different grain sizes varying from 30 to 200 nm were obtained with the change of laser parameters. The calculated activation energy is of 1.13 eV and it was less than the lattice diffusion activation energy. Fick's law and average field method was applied to simulate the laser oxidation kinetics in Cr films. The differential form of homogeneous grain growth formula at equivalent constant temperature was used to establish laser oxidation kinetics. The inverse logarithm relation between oxidation rate and laser acting time was observed when the grain sizes of film were in 100–200 nm and it complied with Wagner theory and the parabola kinetics curve. The oxidation kinetics complied with Carbrea–Mott theory when the oxide film grain sizes were less than 100 nm. Cabrera–Mott oxidation kinetics was applied to not only the grain sizes within 10 nm, but also the grain sizes up to 100 nm. This result filled up the blank in the oxidation kinetics with grains sized of 10–100 nm. These results from the laser enhanced desorption which could reach rather deeper layer in the film under laser oxidation.

Keywords: Laser oxidation; Thin oxide film; Oxidation mechanism; Morphology; Oxidation kinetics

1. Introduction

Over the last four decades of studies on surface oxidation of metals, both coarse crystal metals and monocrystal metals are well-knowledged in oxidation processes, oxidation kinetic, surface morphology and structures. In the former case, the surface modification of Ti [1], Al [2] and Zn [3] has potentially practical application in corrosion inhibition. In the later case, initial oxidation of Ni, Al, Cu, Ti [4–8] as well as Cr [9–14] has been widely studied with STM, LEED, XPS and AES. The considerable detailed information about the nature of physisorption, chemisorption and initial oxidation that are all very important basic aspects of surface science has been obtained.

In contrast to the surface oxidation of coarse crystalline and monocrystal metals, the practical meaning of oxidation of the nanostructural metal films does not only consist in the oxidation resistance of films in service [15–17], but also is considered as a potential method in direct synthesizing some oxide films [18–21]. The films are often synthesized from various vacuum methods such as PVD, CVD, PLD and sol–gel chemical method. The micrometer-scale ordered conducting PdO_2 film has been synthesized from the direct Pd film oxidation for the photoelectron emission application [18]. TiO_2 [19], SnO_2 [20] and SiO_2 [21] were synthesized from the thermal oxidation for ultraviolet ray sensors, gas sensors and CMOS devices. Besides, plasma [22], micro arc [23] and hyperthermal atomic oxygen [24] were proved to be potential methods to synthesize the oxide film.

In previous works, the laser surface processing was concerned with laser deposition (PLD) and laser modification such as laser hardening and annealing. Meanwhile, local laser oxidation was regarded as a considerable method to synthesize directly oxide films [25,26] and maskless photolithographic [27–31]. The fundamental work has been done by

* Corresponding author. Tel.: +86 431 5705875; fax: +86 431 5705876.
E-mail address: jiagzh@jlu.edu.cn (J. Hu).

0921-5093/$ – see front matter © 2004 Elsevier B.V. All rights reserved.
doi:10.1016/j.msea.2004.08.077

Nánai et al. [32] and Metev et al. [28] in the field of nonlinear dynamic and pattern writing resolution of laser oxidation. In recent years, Nd-YAG-laser oxidation has induced the increasing interest in many fields of micro fabrication applications. Huber et al. [27] presented a direct laser-thermal oxidation method for lateral patterning of silicon on insulator (SOI) film with the sub-mm resolution. Haefliger and Stemmer [30] reported that Al-coated aperture scanning near-field optical probes with a protruding silicon nitride tip were fabricated by low-power laser-thermal oxidation in water under common laboratory conditions. Vernold and Milster [29] reported their non-photolithographic fabrication technology (laser oxidation) instead of current state-of-the-art techniques for fabricating large computer-generated diffractive optical elements. Therein, laser oxidation can be divided into two groups: wet method and dry method.

Laser beam has several consequences of wavelength and a higher absorptivity, a lower sensitivity against laser-induced plasmas and, in particular in the uses of flexible glass fibers for beam handling. Simultaneously, disadvantages like poor beam quality and low efficiency has been effectively reduced by recent developments of diode-pumped systems [33]. In addition an autofocus system [27] could provide a constant laser spot size during writing process. All these are helping laser oxidation to become a competitive method in micro fabrication processes.

The oxidation mechanism of the Cr can be explained by the chemisorption. Maurice et al. [34] studied the chemisorption on Cr(1 1 0) by means of XPS, LEED and STM. They investigated the oxygen adsorption and nuclei by dosing about 0.2 L ($1\,L = 1 \times 10^{-6}$ Torr s) of O_2 at 300 and 625 K. At 300 K, a granular and non-crystalline oxide formed, which grew with a constant Cr_2O_3 stoichiometry up to a limiting thickness of 0.9 nm. Thickening at 625 K leads to the formation of a non-crystalline oxide, which grows up to a limiting thickness of 4.6 nm. The presence of Cr^{3+} vacancies related to a significant cation transport through the oxide film in this temperature regime is detected. However, Brown and You [35] observed a quasi-hexagonal primary pattern with an average corrugation amplitude of 3.0 Å. The observed STM topography was consistent with the existence of an ordered chromium sesquioxide (Cr_2O_3) layer having the quasi-hexagonal structure of the air-oxidized Cr(1 1 0) surface. In addition, an atomic step was observed on this naturally oxidized Cr(1 1 0) surface. Palacio et al. [36] investigated the interaction of oxygen with a polycrystalline chromium surface at 300 K in the 10^{-8} to 10^{-6} Torr pressure range. Foord and Lambert [37] observed a well-ordered oxide structure on single crystal Cr(1 1 0), whereas Cr(1 1 0) exhibited oxygen-induced faceting.

For thin films the driving force for mass transport of reactants may be due to electric fields in or across the initial oxide layer and the kinetics leads to the inverse logarithmic law (Cabrera–Mott theory); for thick films, it is determined by the chemical potential gradient across the oxide layer. This leads to a parabolic law of oxidation (Wagner theory). However, the reaction path and the oxidation behavior of a metal may depend on varieties of factors, and the reaction mechanisms were often proved to be complex, some other types of oxidation law, such as linear, cubic and their combinations have been experimentally observed. Nánai et al. [31] has presented the validity region of Cabrera–Mott law at the range of 0–10 nm layers and Wagner law at range of 100–10000 nm using Ni at 500 °C as an example.

Whereas, the laws that occur and the changes that take place at the metal film surface, in the formation and growth of oxide film by the pulsed laser irradiation are still poorly understood, even for a simple system such as Cr/Cr_2O_3 considered in this study. There is still a need of fundamental knowledge of the relationships between the oxide film growth mechanism and the oxidation kinetics, morphology and microstructure of the developing oxide film by pulsed laser irradiation. The problem is that the thermal filed produced by pulse laser irradiation during oxidation of metal film is variable and transient; whereas, the oxidation kinetic laws (Wagner theory or Cabrera–Mott theory) are based on a definite temperature or temperature range. Variable temperature profiles are not easy to be employed to build the oxidation kinetics in the laser oxidation condition.

In the present paper, the Cr thin film obtained through vacuum evaporation was oxided by Nd-YAG pulse laser and the influences of laser energy on the morphology and grain size of Cr oxide were studied. For the theoretical analysis, the Fick's I law and the average field method were applied to simulate the laser oxidation kinetics in Cr films. The differential form of homogeneous grain growth formula at equivalent constant temperature was used in the study of laser oxidation kinetics. Both the Carbrea–Mott theory and the Wagner theory were used in the analyses of the oxidation kinetics of Cr film under different laser energy density. The purpose of the present work was to illustrate that the classical oxidation kinetics theories (both the Carbrea–Mott theory and the Wagner theory) were also applicable to the laser oxidation condition. It may offer a favorable academic tool for the study of non-stable oxide process.

2. Experiments

Polycrystalline Cr films with a thickness 2 μm were deposited thermally on grown $SiO_2/Si(1\,1\,1)$ substrates from a high purity polycrystalline Cr evaporated through electron bombardment. UHV conditions were kept throughout the evaporations with chamber pressures in the 10^{-4} Pa range. The temperature of substrates was kept at 200 °C during deposition to improve the adhesion between the Cr film and the substrate. A Nd-YAG laser with 1062 nm wavelength was used. Samples were mounted on a computer-controlled *X*–*Y* stage to allow their displacement under the laser beam with pre-set scan velocity in order to increase the oxidation area. Typically, the laser beam with a spot size of 200 μm diameter was under focus on the sample surface in air. The laser energy from 15 to 100 mJ was applied. The YAG energy meter was

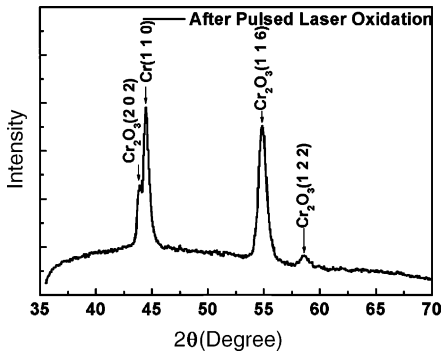

Fig. 1. Low-angle XRD patterns of Cr_2O_3 after laser oxidation.

employed to measure the laser spot energy. For comparison, as-deposited Cr film samples were annealed for 15 min in air condition at 600, 700, and 800 °C in furnace to form Cr_2O_3 film. The surface morphology was studied with SEM, FESEM and AFM. Au layers with about 30 Å thickness were deposited on every sample by ion sputter for the sake of improvement of electric conductivity for SEM observation. Structure analysis was performed by X-ray diffraction (XRD) measurements with a D8 Discover diffractometer ($\lambda = 1.54$ Å). Low-angle scan mode was performed to limit X-ray penetration depth at the region near the oxide film surface.

3. Results and discussion

3.1. Surface microstructure of Cr film by the laser oxidation

The grain size of as-deposited Cr film was about 10 nm from our previous study and Cr films grew and formed (1 1 0) texture [38], since the surface energy is the smallest at the (1 1 0) plane in bcc [39]. Our investigation also showed that after the laser irradiation only Cr_2O_3 was detected by XRD while no other sorts of chromium oxide was found (see Fig. 1 of the XRD results). The surface morphology and the grain size of oxide were investigated by SEM and FESEM, which shows that grains grew after the laser irradiation, the grain sizes increase with the laser energy increasing. Fig. 2a–c showed that after laser irradiation with laser energy in the range of 15–27.5 mJ and the pulse duration of 0.1 ms, oxide grains grew to 10–100 nm. Fig. 2d–f showed that after the irradiation of 30–100 mJ, 1 ms laser, grains grew to 110–200 nm. The relationship between laser power density and the grain size of oxide was shown in Fig. 3.

AFM study showed that after laser irradiation with 0.1 ms pulse duration, the surface oxide direction of growth is upwards. The typical cone structure formed was about 6–10 nm high (Fig. 4a). However, after 1 ms pulse duration laser irradiation, the surface oxide grew laterally and the short plateau structure formed with 5 nm high, then the groove structure formed (Fig. 4b). So we believed that the upward growth of oxide slowed down gradually, but the lateral growth still existed.

3.2. Comparison experiments: oxygen annealing of polycrystalline Cr film

The surface morphology of Cr film after annealed in air at 600 °C for 15 min was shown in Fig. 5a. The average grain size was about 100 nm. The film surface was relatively flat and no wrinkle structure formed. The surface morphology of Cr film after annealed in air at 700 °C for 15 min was shown in Fig. 5b. The average grain size was about 180 nm. The surface oxide showed the typical faceting structure, but no wrinkle formed because the low oxidation rate builds the lower growth stress. In this condition surface oxide layers were still compact and had no pore. Whereas the surface morphology of Cr film after annealed in air at 800 °C for 15 min was shown in Fig. 5c. The average grain size was about 350 nm. The film surface appears the obvious wrinkle structure (Fig. 5d low magnifies). Because the deeper oxidation formed at the higher temperature could build the higher stress. The relaxation of stress results in the formation of wrinkle structure. Often, inhomogeneous growth will form some pores at the edges of the wrinkle.

3.3. Oxidation mechanism of Cr_2O_3

The total chemical reaction for the reaction of a metal M and oxygen gas O_2 to form oxide may be written as:

$$aM + \frac{b}{2}O_2 = M_aO_b \tag{1}$$

For the Cr/O_2 system, this reaction is written as:

$$\frac{4}{3}Cr + O_2 = \frac{2}{3}Cr_2O_3 \tag{2}$$

From this equation the oxidation of metals may seem to be among the simplest chemical reaction. The driving energy of this metal–oxygen reaction is free energy change associated with the formation of the oxide from the reactants. The oxide will form only if the ambient oxygen pressure is larger than the dissociation pressure of the oxide in equilibrium with the metal, that is:

$$p_{O_2} \geq \exp\left[-\frac{2\Delta G^0(M_aO_b)}{bRT}\right] \tag{3}$$

where

$$\Delta G^0(Cr_2O_3) = -746844\,(J\,mol^{-1}) + 173.2\,(J\,mol^{-1}\,K^{-1})T \tag{4}$$

It is clearly that for almost all metals such as Fe, Ni, Cr, Ti and Al, values of ΔG^0 are negative at air condition in temperature range of 298–1868 K. That is to say reaction (1) posses the spontaneity. So that initial oxidation will start at an absolutely clean surface in this condition.

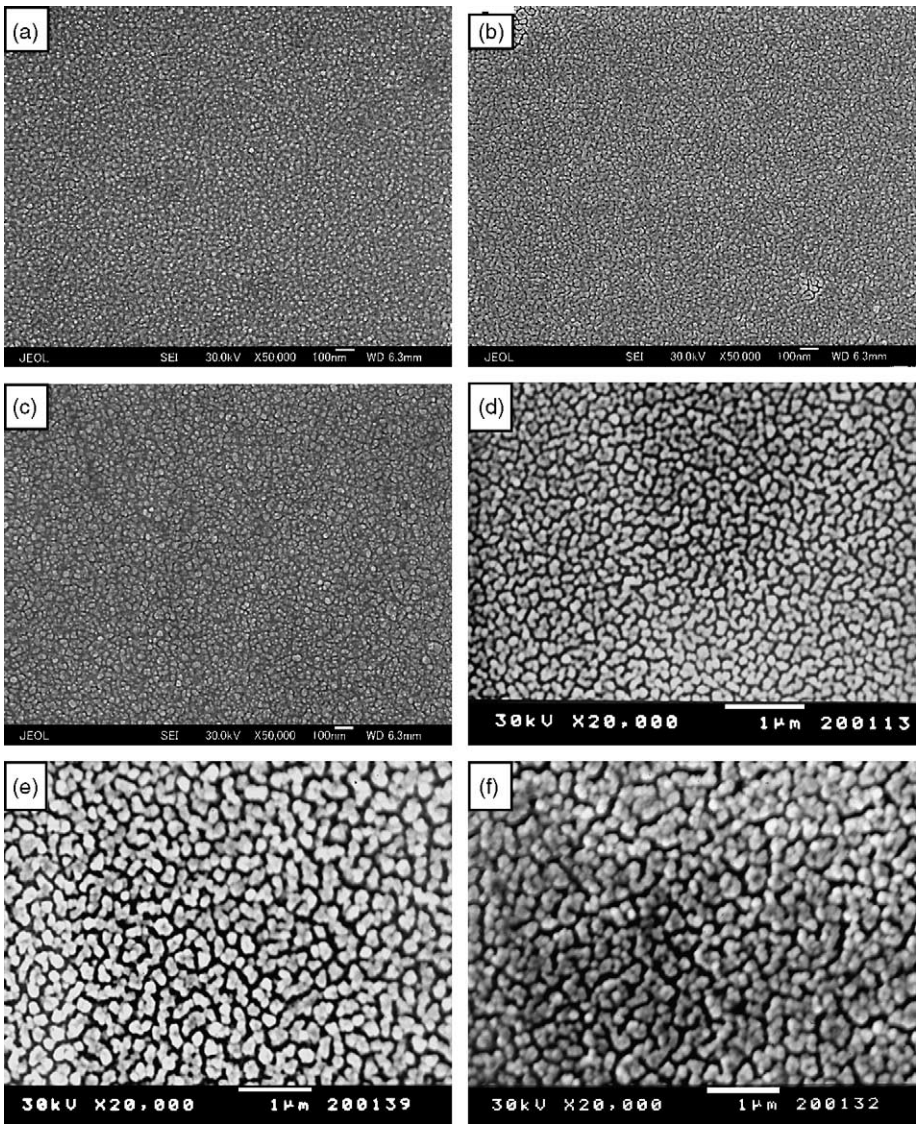

Fig. 2. FESEM and SEM surface micrograph of Cr film (a) 15 mJ, 0.1 ms laser irradiation. The grain size was 15 nm. (b) 20 mJ, 0.1 ms laser irradiation. The grain size was 30 nm. (c) 22.5 mJ, 0.1 ms laser irradiation. The grain size was 50 nm. (d) 70 mJ, 1 ms laser irradiation. The surface oxide film was smooth and the grain size was 120 nm and the grain adhesion appeared. (e) 90 mJ, 1 ms laser irradiation. The surface oxide film was smooth and the grain size was 160 nm and the further grain adhesion appeared. (f) 100 mJ, 1 ms laser irradiation. The surface oxide film was smooth and the grain size was 200 nm and the further grain adhesion appeared.

The initial oxidation mechanism of the Cr can be explained by the chemisorption:

1. The non-crystalline chemisorption nuclei are formed with a constant Cr_2O_3 stoichiometry on the clean surface Cr(1 1 0) with the higher vacuum and the lower oxygen exposures at the room temperature.
2. The crystalline Cr_2O_3 film formed on the clean surface Cr(1 1 0) with the higher vacuum, oxygen exposures or the atmosphere condition at the room temperature.
3. At the lower oxygen partial pressure, nucleation of Cr_2O_3 islands which grow laterally on Cr(1 1 0) shows the anisotropy; at the higher oxygen partial pressure, the growth of Cr_2O_3 shows isotropy and exhibited oxygen-induced faceting.

Therefore, the initial oxide layer separates the metal Cr from the oxygen gas. Deeper reaction can proceed only by the solid-state diffusion of the reactants through the previously formed oxide layer.

From the oxidation kinetics study of Cr(1 1 0) by Stierle and Zabel [40], an overall activation energy of 1.4 eV for diffusion of Cr through Cr_2O_3 layer was determined, which is much smaller than the value of 2.9 eV for diffusion via buck interstitial sites. From our experimental data (Table 1) of Cr film oxidation in furnace surface the oxide grain grew from 10 to 100 nm, 180 and 350 nm at 873, 973 and 1073 K, re-

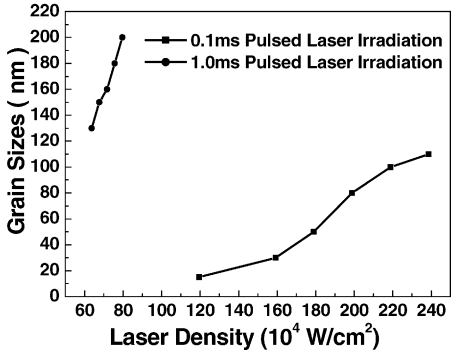

Fig. 3. Relationship between laser power density and grain sizes of oxide.

Table 1
Experimental data of annealed oxidation ($d_0 = 6$ nm, $\Delta t = 900$ s)

Oxidation temperature (K)	Grain sizes (nm)	Symbol
873	100	d_1
973	180	d_2
1073	350	d_3

spectively. Calculated from the Eq. (12) or from the graphic method (Fig. 6), we could gain the solution of activation energy E of 1.13 eV.

3.4. Transient thermal field by laser oxidation

The film surface heating caused by an incident laser pulse is due to electronic excitation processes accompanying the absorption of light. In our experiment the pulse duration of 0.1–1 ms far exceed the relaxation time for electronic transitions ($\approx 10^{-12}$ s). The fundament thermal equation [43] for the temperature $T(x, t)$ that to be solved is:

$$\rho c \frac{\partial T(x,t)}{\partial t} - \kappa \frac{\partial^2 T(x,t)}{\partial x^2} - A(x,t) = 0, \quad 0 < x < \infty \tag{5}$$

where the first two terms representing conventional one-dimensional heat conduction. The term $A(x, t)$ in units of W/cm^3, is the spatial and time-dependent power density absorbed from the incident laser pulse. Hence, we assume that $A(x, t)$ can be written as

$$A(x,t) = I_0 A \delta(x-0) H(t-\tau) \tag{6}$$

According to the boundary conditions concerns heat transfer through the surface given in [42]. Closed-form solutions for both transients heating and cooling can be obtained by Laplace transform methods. During heating ($t < \tau$), the solution is:

$$T(x,t) = T_h(x,t) = \frac{I_0 A}{\kappa}\left[\sqrt{\frac{4Kt}{\pi}}\,\exp\frac{-x^2}{4Kt} - x \times \operatorname{erfc}\frac{x}{\sqrt{4Kt}}\right] + T_0 \tag{7}$$

During cooling the temperature drops for all $t > \tau$ and

$$T(x,t) = T_c(x,t) = \frac{I_0 A}{\kappa}\sqrt{4K} \times \left[\sqrt{t} \times \operatorname{ierfc}\frac{x}{\sqrt{4Kt}} - \sqrt{t-\tau} \times \operatorname{ierfc}\frac{x}{\sqrt{4K(t-\tau)}}\right] + T_0 \tag{8}$$

where

$$\operatorname{ierfc}(z) = \int_z^\infty \operatorname{erfc}(y)\,dy = \frac{1}{\sqrt{\pi}} e^{-z^2} - z \times \operatorname{erfc}(z)$$

where Q is pulse energy (J), P is pulse power (W), A is the absorption coefficient of Cr film, ω is laser spot radius, x is the distance measured from the surface, I_0 is power density (W/m^2) and I is the effective power density of laser spot ($I = I_0 A$).

Eqs. (7) and (8) represent the surface temperature variation during its heating and cooling, respectively. The heating process by laser irradiation was calculated by Eq. (7) from time 0 to pulse time τ. Then after the pulse, the cooling process was calculated by Eq. (8). A group of temperature variation curves calculated by Eqs. (7) and (8) for different laser energy density were shown in Fig. 7. It is seen that the temperature on Cr film surface increases with increasing laser energy. If

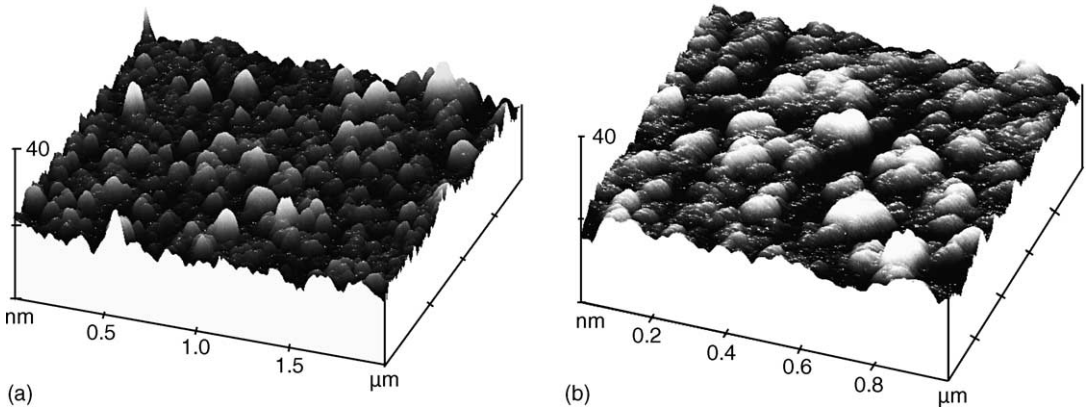

Fig. 4. AFM 3-D image of Cr film surface after laser irradiation. (a) The laser energy is 25 mJ at 0.1 ms pulse duration. (b) The laser energy is 80 mJ at 1 ms pulse duration. Groove structure was found.

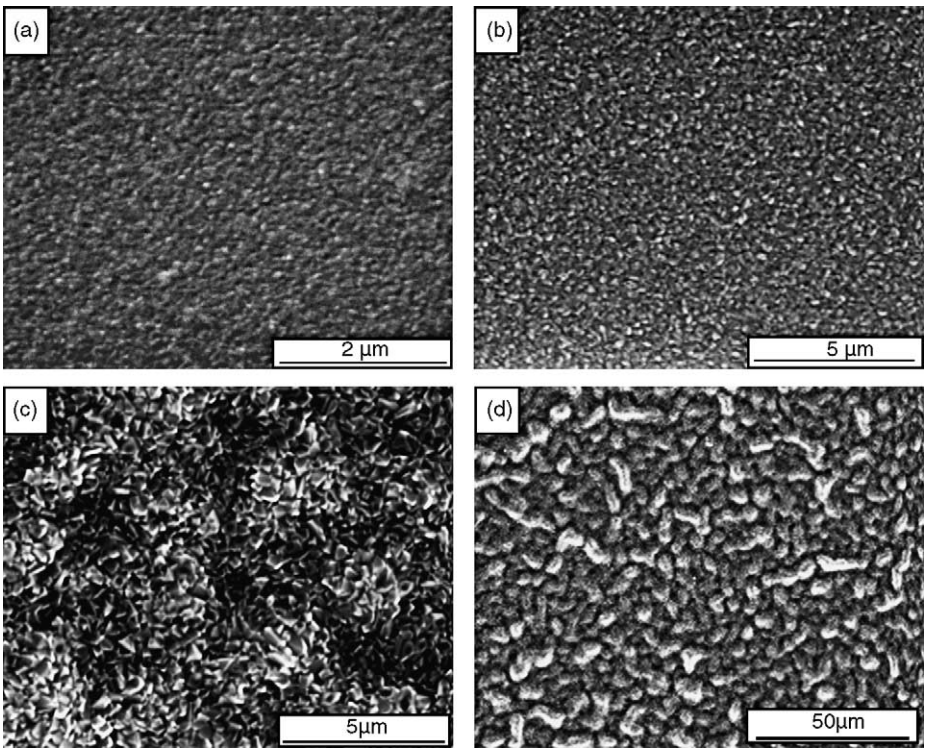

Fig. 5. SEM micrograph of Cr film annealed oxidation in furnace (a) 600 °C for 15 min in air. (b) 700 °C for 15 min in air. (c) 800 °C for 15 min in air. (d) Wrinkle micrograph at 800 °C for 15 min in air low magnification.

the oxidation of Cr film is assumed to take place above a certain temperature (e.g., 500 °C), the oxidation duration also increases with increasing laser energy. For the further analysis of the oxidation kinetics of Cr film by laser irradiation, it is better to simulate the temperature curves in an analytic formation. It was found that the Lorentz curve fit the temperature versus time curves well. The Lorentz fit equation is:

$$T(t) = T_0 + \frac{2A}{\pi} \times \frac{\omega}{4(t - t_c)^2 + \omega^2} \tag{9}$$

where T_0, A, ω and t_c are fit parameters. Fig. 8 shows that as-fitted curves (dark lines) well accorded with the corresponding solution curve (black line), and the Lorentz parameters were listed in Table 2.

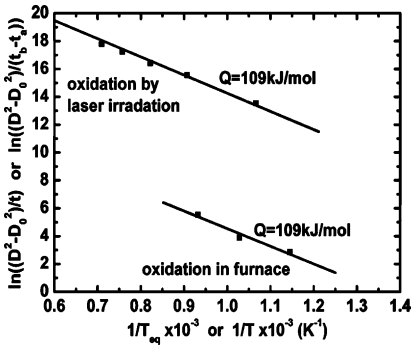

Fig. 6. The solution of activation energy E of 1.13 eV or from graphic method.

3.5. Simulation of grain growth during oxidation

In our previous work [38], laser oxidation Cr film was studied and obvious grain growth was found in the oxidation process that depended on the applied laser energy. The grain growth after oxidation of Cr to Cr_2O_3 is also a thermal

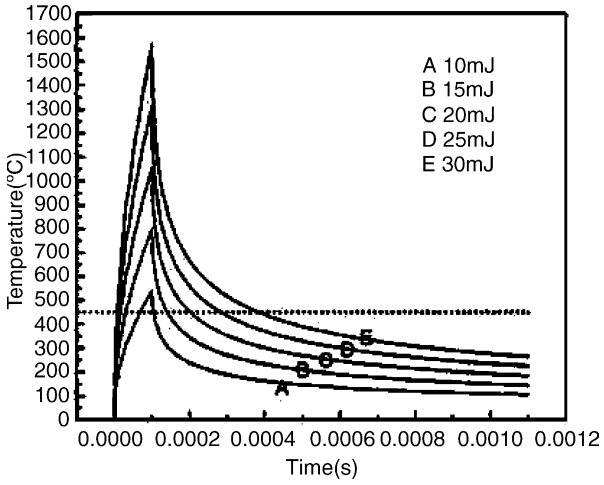

Fig. 7. The temperature curve of Cr films surface varying with the different pulsed laser energy irradiation.

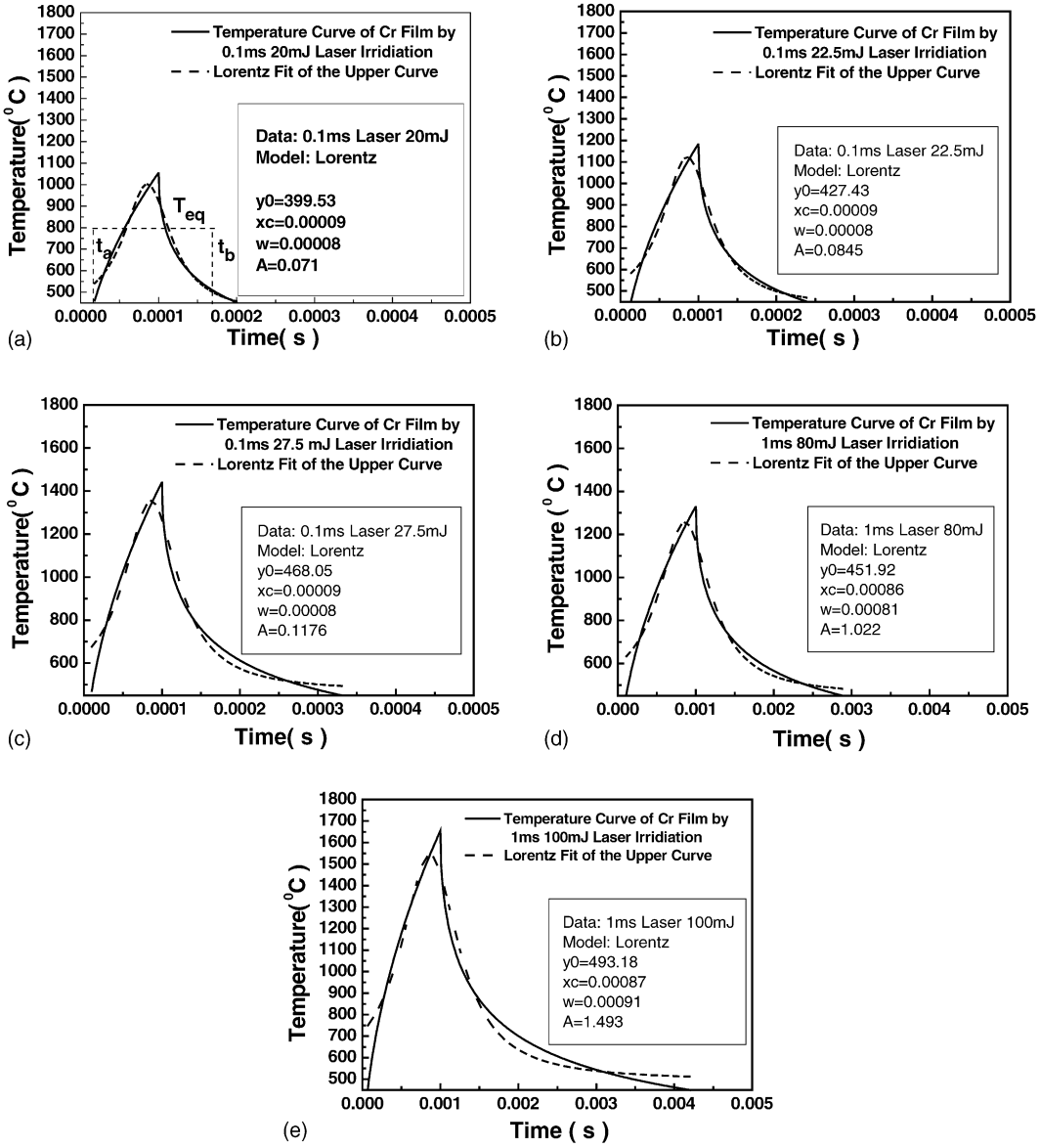

Fig. 8. Lorentz fit of surface thermal field, (a) 20 mJ, (b) 22.5 mJ, (c) 27.5 mJ, (d) 80 mJ and (e) 100 mJ.

Table 2
Parameters for calculation of grain growth at equivalent temperature of 800 °C

Laser energy (W/cm^2) ($\times 10^4$)	Parameters of fit Lorentzin				t_a (10^{-4} s)	t_b (10^{-4} s)	$\int_{t_a}^{t_b} e^{-E/RT(t)}$ (10^{-10})	Δt^*_{eq} (10^{-4} s)	x (nm)	x^{-1} (10^7 nm^{-1})
	T_0	t_c (10^{-5})	ω (10^{-5})	A						
119	324.3	9	7	0.05	0.31	1.40	1.13	0.23	15	6.67
159	399.5	9	8	0.07	0.18	2.00	8.35	1.7	30	3.33
179	427.4	9	8	0.08	0.14	2.39	20.00	4.07	50	2.00
199	449.2	9	8	0.10	0.11	2.83	64.88	13.22	80	1.25
219	468.1	9	8	0.12	0.10	3.31	163.00	33.2	100	1.00
239	484.1	9	9	0.14	0.08	3.83	233.20	47.5	110	0.90
64	451.9	86	81	1.02	1.1	28.8	690.90	140	130	0.77
68	463.9	86	83	1.13	1.0	31.8	1077.00	220	150	0.67
72	474.6	86	86	1.25	0.9	35.0	1582.00	320	160	0.60
76	484.3	86	88	1.37	0.8	38.4	2290.00	470	180	0.56
80	493.2	87	91	1.49	0.7	42.0	3063.00	620	200	0.50

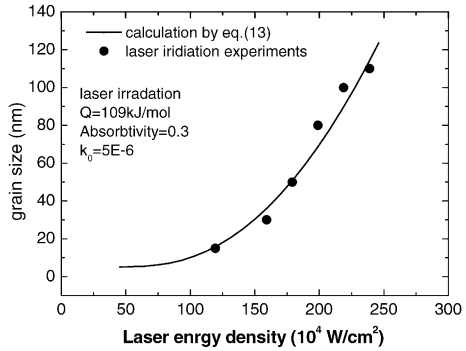

Fig. 9. Relation of grain size vs. laser energy density, comparison between simulation and experiments.

diffusion process. Therefore, classical grain growth equation based on thermal diffusion [44] was used to approach the grain growth during laser oxidation of Cr film:

$$D_t^2 - D_0^2 = k_0 \exp\left(-\frac{E}{RT}\right) \mathrm{d}t \tag{10}$$

where D_0 and D_t are the grain sizes of Cr_2O_3 at the beginning of the experiment and at time t, respectively. R is the molar gas constant and k_0 is a constant that is independent of the absolute temperature T. E is the activation energy for isothermal grain growth. From a phenomenological view, E is often used to determine the microscopic mechanism of grain growth.

In fact, Eq. (10) accounts for the isothermal grain growth at a constant temperature. For the grain growth of oxide during laser irradiation, the temperature filed $T = T(t)$ (see Fig. 7 or 8) can be simply described by Eq. (9). Therefore, a variable temperature should be introduced in the grain growth model. In the present cases, it was found that the following integral form can be reasonably applied:

$$D_t{}^2 - D_0^2 = k_0 \int_{t_a}^{t_b} \exp\left(-\frac{E}{RT(t)}\right) \mathrm{d}t \tag{11}$$

where $T(t)$ described by Eq. (9) is a function of time. If a low temperature limit is assumed, under it there is no evident grain growth, then t_a and t_b are the start and end times of grain growth of oxides, respectively (shown by Fig. 8a). Because there is no clear grain growth of oxide by laser irradiation with the laser energy of 10 mJ, the low limit temperature is taken as 500 °C. For different laser energy density, the values of t_a and t_b were shown in Table 2. Taking the measured value of 1.13 eV by oxygen annealing as the activation energy value, and a value of 0.3 is the absorption coefficient, the grain growth was calculated with Eq. (11). The calculated grain sizes for different energy densities were shown in Fig. 9, in comparison with the experimental ones. Therefore, the grain growth of Cr oxide during pulse laser irradiation on Cr film can be simply simulated by the general grain growth model with a variable temperature.

3.6. Surface oxidation kinetics of Cr film by Nd-YAG laser

3.6.1. Equivalent time temperature and oxidation time

If we assume that the evident oxidation and the grain growth occur above 500 °C and take into account the Lorentz fit of the real temperature variation, from Eq. (11), we can calculate the equivalent temperature T_{eq}, which gives the grain size being in coincidence with the corresponding experimental ones. However, for consideration of oxidation mechanism, a certain temperature should be used for comparison. Combination of Eqs. (10) and (11), one has:

$$D_t^2 - D_0^2 = k_0 \int_{t_a}^{t_b} \exp\left(-\frac{E}{RT(t)}\right) \mathrm{d}t = k_0 \exp\left(-\frac{E}{RT_{eq}}\right) \Delta t \tag{12}$$

where T_{eq} is the equivalent temperature and $\Delta t = t_b - t_a$. The meaning of T_{eq} is that it gives the same grain growth as the one calculated with variable temperature ($T(t)$). If we use T_{eq} as the laser oxidation temperature for different energy, the plotting of $\ln[(D^2 - D_0^2)/(t_b - t_a)]$ via $1/T_{eq}$ also gives the same activation energy value as that obtained by annealing oxidation (109 kJ/mol or 1.13 eV), see Fig. 6. It means that the equvalent temperature approach is self-consistent.

For our experiments of oxidation of Cr, it was found that all the T_{eq} were in the range of 500–1150 °C. Therefore, for the sake of simplicity, we further assumed a stable temperature of 800 °C as the equivalent temperature (T^*_{eq}) for all laser energy density, at which Cr oxidation occurs. From this, we could obtain a series of simulation data of equivalent duration (Δt^*_{eq}), which also gives nearly the same grain sizes as the experimental ones, that is:

$$D_t^2 - D_0^2 = k_0 \int_{t_a}^{t_b} \exp\left(-\frac{E}{RT(t)}\right) \mathrm{d}t = k_0 \exp\left(-\frac{E}{RT^*_{eq}}\right) \Delta t^*_{eq} \tag{13}$$

The resulting Δt^*_{eq} are shown in Table 2. These values of Δt^*_{eq} will be used latter for the analysis of oxidation kinetics mechanism.

During oxidation of Cr film, once a completely dense films form, the deep oxidation will be inhibited because short-circuit diffusion paths vanish. Cr grain boundaries are pinned and could not migrate again. The oxide layer, therefore, is considered as a monolayer. From this deduction, the surface oxide film thickness x is assumed to be equal to the surface oxide grain sizes. That is to say, grain growth kinetics could reflect oxidation kinetics as a linear dependent relation. So we could obtain a kinetics relationship of grain sizes with equivalent time, Δt^*_{eq} at an assumed temperature T^*_{eq}, (see Fig. 10). It includes a rapid oxide growth stage following by a slowly raising stage. The slowly raising stage can be fitted

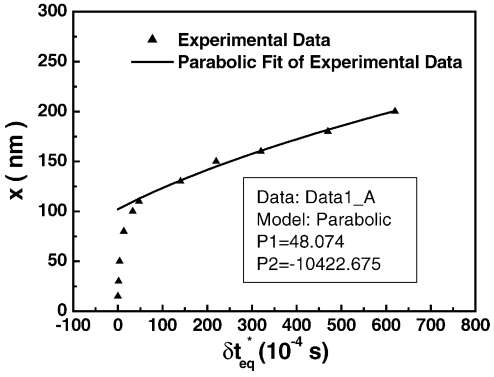

Fig. 10. Non-linear curve fit of oxidation rate and effective time.

by a normal parabolic relation:

$$x^2 = 1011.45t + 5701.04 \tag{14}$$

However, the first rapid growth stage can be well fitted by an inverse logarithmic curve shown by the equation:

$$\frac{1}{x} = -1.04\ \ln(t) + 4.29 \tag{15}$$

So we concluded that there are two distinguishing mechanisms which is dominant for different grain size regions. For grain sizes smaller than 100 nm, the inverse logarithmic law works (Fig. 11), and when grain sizes are larger than 100 nm, the parabolic law plays a main role (Fig. 10).

3.6.2. Cabrera–Mott law and Wagner law

The oxide incorporated into the metallic substrates is a chemically heterogeneous process, which in a classical treatment can be described by the Cabrera–Mott theory for thin oxide films and Wagner theory for thick films. The fundamental concepts are based on the fact that the diffusing species are electrically charged, and thus their flux is determined by the gradient in the chemical potential and the electric fields [31]. As the previous research work, the deep oxide growth must be accomplished by the diffusing species transforming across the initial oxide layer (chemisorption oxide layer), the diffusion flux is expressed as the Fick law. The rate of oxide growth, theoretically, depends on a flux of ions, J, across the oxide overlayer, which can be expressed by a general equation [45]:

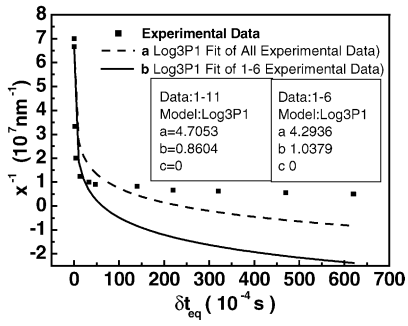

Fig. 11. Non-linear fit of experimental data proved the inverse logarithmic law.

$$J = -D\frac{\mathrm{d}c}{\mathrm{d}x} + cv \tag{16}$$

where D is the diffusion coefficient, c is the concentration and ν is the drift velocity of an ion, which is the diffusing species in the oxide overlayer. The first term in the right-hand side of Eq. (16) is the Fick's first law and the other derives from the Ohm's law. These describe the motion of an ion or charged species in the oxide over-layer under its concentration gradient dc/dx and electrostatic field F, respectively. The electrostatic field, following the Cabrera–Mott theory of low-temperature oxidation is provided by a constant contact potential V created by ionized adsorbed oxygen atoms at the oxide/gas interface. If x is the oxide film thickness, the field strength is given by:

$$F = \frac{V}{x} \tag{17}$$

The drift velocity is proportional to the electrostatic field:

$$u = \mu F_{\mathrm{M}} \tag{18}$$

where μ is the ion mobility. For very thin oxide films, i.e. x is very small, the electrostatic field becomes very strong; e.g. for a film 5 nm thick the field can be the order of 10^7 V/cm and the chemical gradient dc/dx becomes negligible, that is dc/d$x \approx 0$. Under these conditions, the concentration gradient has no effect or can be neglected in the ion flux and the electrostatic field is the only driving force for the ion diffusion. From this deduction, the kinetics relation only at the Mott field as driving force can be expressed as followed [45]:

$$\frac{1}{x} = -\frac{1}{x_{hf}}\ \ln(t) + C \tag{19}$$

where C is a constant and x_{hf} is the limit of Mott field existence

$$x_{hf} = \frac{qaV}{k_{\mathrm{B}}T} \tag{20}$$

where q is an electric charge, a is the interatomic jump distance in the oxide overlayer and k_{B} and T have the usual meanings. On the contrary, when oxide layers are thick, the chemical potential driving force is much stronger than that from Mott field. So that diffusing flux Eq. (16) can be expressed only by the first term. That is to say, the main driving force is the chemical potential. In this condition, the parabolic law can be deduced as the formation of the classic Wagner oxidation theory [41]. Many metal oxidation kinetics accorded with the Wagner oxidation theory, and could be described by the normal parabolic law [46].

In our cases, two distinct mechanisms operates, the Cabrera–Mott law is better applicable in the range of grain sizes less than 100 nm, and the Wagner law operates for grain sizes larger than 100 nm. The former results are rather differ-

ent from the normal oxidation results, where Cabrera–Mott oxidation occurs only within oxidation layer thickness (or grain size) less than 10 nm. The difference can be explained by the particularity of laser oxidation. It may have two possible reasons accounting for this phenomenon. One is the defect production by the laser irradiation and the other is the laser-induced desorption of the initial chemisorption layers.

As we all know that polycrystalline metal films contain dislocations, grain boundaries, and external surfaces. Diffusion along these defects and surface defects is more rapid than the diffusion of atoms in the crystal lattice. Although direct quantitative measurements of diffusion along line and surface defects are experimentally more difficult to perform than those of lattice diffusion, the available data showed that the diffusion coefficients for short circuit diffusion are 1.3–2 times larger than the lattice diffusion coefficients [47]. In our experiments, an overall activation energy 1.13 eV for diffusion of Cr through Cr_2O_3 layer was determined, which is much smaller than the value of 2.9 eV for diffusion via buck interstitial site. This low activation energy means that grain boundary or film surface diffusion is the main mechanism. This sort of short circuit diffusion make it possible that Cr film could be oxidized even in the short duration heating by the laser irradiation.

4. Conclusion

From the experimental research on the oxidation of Cr film by pulse laser and the theoretical analysis on grain growth oxidation kinetic mechanism, conclusions were drawn in this paper. The calculated activation energy by annealing experiments is 1.13 eV (109 kJ/mol) and it was much less than the lattice diffusion activation energy. The Fick's law and the average field method were applied to simulate the laser oxidation kinetics in Cr films. The differential form of homogeneous grain growth formula was used to simulate the grain growth and to establish the laser oxidation kinetics. We had found that oxidation kinetics complied with the Carbrea–Mott theory when the oxide film grain sizes were less than 100 nm. There was the relation of inverse logarithm between the oxidation rate and the laser acting time. However, when grain sizes were 100–200 nm, it complied with Wagner theory and the kinetics curve has the parabola form. The theory accorded with the experiment data.

It indicated that Cabrera–Mott oxidation kinetics was applied to not only the grain sizes within 10 nm, but also the grain sizes up to 100 nm. This result filled up the blank in the oxidation kinetics with the grains sized of 10–100 nm. We deduced that this result was related to the laser enhanced desorption which could reach the rather deeper layer in the film under laser oxidation. In the end, we could speculate that classical oxidation kinetics theory were also applicable to the laser oxidation condition. It may offer a favorable academic tool for the study of rapid and non-equilibrium oxide process.

References

[1] G. Lu, L.B. Steven, J. Schwartz, Surf. Sci. 458 (2000) 80.
[2] V.K. Tolpygo, D.R. Clarke, Mater. Sci. Eng. A278 (1999) 142.
[3] R K. Gupta, S.N. Hridhar, M. Katiyar, Mater. Sci. Semicond. Process. 5 (2002) 11.
[4] R. Domnick, G. Held, H.P. Steinrück, Surf. Sci. 516 (2002) 95.
[5] A. Kiejna, B.I. Lundqvist, Surf. Sci. 504 (2002) 1.
[6] Y.G. Hao, B.R. Cooper, Surf. Sci. 312 (1994) 250.
[7] J. Harris, B. Kasemo, E. Törnqvist, Chem. Phys. Lett. 52 (1977) 538.
[8] B. Singh, J. Müller, N.A. Surplice, Thin Solid Films 21 (1974) 255.
[9] J.S. Foord, M. Lambert, Surf. Sci. 161 (1985) 513.
[10] Y. Sakisaka, H. Kato, M. Onchi, Surf. Sci. 120 (1982) 150.
[11] G. Gewinner, J.C. Peruchetti, A. Jaegle, A. Kalt, Surf. Sci. 78 (1978) 439.
[12] N.D. Shinn, Surf. Sci. 214 (1989) 174.
[13] E.P. Gusev, A.P. Popov, Surf. Sci. 248 (1991) 241.
[14] M.D. Brown, H.X. You, Surf. Sci. 233 (1990) 317.
[15] J.S. Lin, H. Cabibil, B. Ekstrom, J.A. Kelber, Surf. Sci. 371 (1997) 337.
[16] M.C.G. Passeggi Jr., L.I. Vergara, S.M. Mendoza, J. Ferrón, Surf. Sci. 507–510 (2002) 825.
[17] S.V. Metelev, N.K. Pleshanov, A. Menelle, V.M. Pusenkov, A.F. Schebetov, Z.N. Soroko, V.A. Ul'yanov, Phys. B Condens. Matter 297 (2001) 122.
[18] S. Aggarwal, A.P. Monga, S.R. Perusse, R. Ramesh, V. Ballarotto, E.D. Williams, B.R. Chalamala, Y. Wei, R.H. Reuss, Science 287 (2000) 2235.
[19] K.S. Lee, I.S. Park, Scr. Mater. 48 (2003) 659.
[20] A. Karthigeyan, R.P. Gupta, M. Burgmair, S.K. Sharma, I. Eisele, Sen. Actuat. B Chem. 87 (2002) 321.
[21] P. Mur, M.N. Semeria, M. Olivier, A.M. Papon, Ch. Leroux, G. Reimbold, P. Gentile, N. Magnea, Appl. Surf. Sci. 175/176 (2001) 726.
[22] K. Draou, N. Bellakhal, J.L. Brisset, B.G. Chéron, Mater. Chem. Phys. 51 (1997) 142.
[23] G.L. Yang, X.Y. Lü, Y. Bai, H. Cui, Z. Jin, J. Alloys Compounds 345 (2002) 196.
[24] F.W. Jason, T.J. Campbell, G.B. Hoflund, G.N. Salaita, J. Electron. Spectrosc. Relat. Phenomena 106 (2000) 81.
[25] S. Sasa, T. Ikeda, C. Dohno, M. Inoue, Physica. E 2 (1998) 858.
[26] E. György, A. Pérez del Pino, P. Serra, J.L. Morenza, Appl. Surf. Sci. 197/198 (2002) 851.
[27] M. Huber, R.A. Deutschmann, R. Neumann, K. Brunner, G. Abstreiter, Appl. Surf. Sci. 168 (2000) 204.
[28] S.M. Metev, S.K. Savtchenko, K.V. Stamenov, J. Phys. D Appl. Phys. 13 (1980) 75.
[29] C.L. Vernold, T.D. Milster, Proc. SPIE 2263 (1994) 125.
[30] D. Haefliger, A. Stemmer, Microelectron. Eng. 61/62 (2002) 523.
[31] L. Nànai, R. Vajtai, T.F. George, Thin Solid Films 298 (1997) 160.
[32] L. Nànai, R. Vajtai, T.F. George, Infrared Phys. Technol. 36 (1995) 281.
[33] H. Hügel, Opt. Lasers Eng. 34 (2000) 213.
[34] V. Maurice, S. Cadot, P. Marcus, Surf. Sci. 458 (2000) 195.
[35] N.M.D. Brown, H.X. You, Surf. Sci. 233 (1990) 317.
[36] C. Palacio, H.J. Mathieu, D. Landolt, Surf. Sci. 182 (1987) 41.
[37] J.S. Foord, M. Lambert, Surf. Sci. 161 (1985) 513.
[38] Q. Dong, J.D. Hu, J.S. Lian, Z.X. Guo, J.W. Chen, B. Chen, Scr. Mater. 48 (2003) 1373.
[39] K.S. Park, J.K. Park, Acta Mater. 47 (1999) 2177.
[40] A. Stierle, H. Zabel, Surf. Sci. 385 (1997) 167.
[41] P. Kofstad, High Temperature Corrosion, Elsevier Applied Science Publishes Ltd., 1988, p. 75.
[42] J.L. Jiménez Pérez, P.H. Sakanaka, M.A. Algatti, J.G. Mendoza-Alvarez, A. Cruz Orea, Appl. Surf. Sci. 175/176 (2001) 709.

[43] M. Ohring, The materials science of thin films, Chapter 13, in: Modification of Surfaces and Films, Academic Press, 2002, p. 596.
[44] J.S. Lian, R.Z. Valiev, B. Baudelet, Acta Metall. Mater. 43 (1995) 4165.
[45] T. Do, N.S. McIntyre, Surf. Sci. 440 (1999) 438.
[46] K.M. Latt, Y.K. Lee, T. Osipowicz, H.S. Park, Mate. Sci. Eng. B94 (2002) 111.
[47] J.M. Poate, K.N. Tu, J.W. Mayer, Thin Film Interdiffusion React. (1978) 127.